Adsorption (2024) 30:107–119
https://doi.org/10.1007/s10450-023-00435-6

Breakthrough analysis of the CO_2/CH_4 separation on electrospun carbon nanofibers

Victor Selmert[1,2] · Ansgar Kretzschmar[1] · Hans Kungl[1] · Hermann Tempel[1] · Rüdiger-A. Eichel[1,2]

Received: 21 June 2023 / Revised: 13 December 2023 / Accepted: 18 December 2023 / Published online: 4 February 2024

Abstract
The removal of the main impurity CO_2 is a crucial step in biogas upgrading. In this work, the separation of CO_2 from CH_4 on electrospun polyacrylonitrile-based carbon nanofibers (CNFs) is investigated using breakthrough experiments. The CNFs are prepared at various carbonization temperatures ranging from 600 to 900 °C and feature a tailorable pore size that decreases at higher carbonization temperatures. The adsorption properties of the different CNFs are studied measuring pure component isotherms as well as column breakthrough experiments. Adsorption kinetics are discussed using a linear driving force approach to model the breakthrough experiment and obtain the adsorption rate constant. Moreover, different approaches to determine the selectivity of the competitive CO_2/CH_4 adsorption are applied and discussed in detail. The results clearly prove that a size exclusion effect governs the adsorption selectivity on the CNFs. While CH_4 cannot adsorb in the pores of CNFs prepared at 800 °C or above, the smaller CO_2 is only excluded from the pores of CNFs prepared at 900 °C. For CNFs carbonized in the range from 600 to 750 °C, values of the CO_2/CH_4 selectivity of 11–14 are obtained. On the CNFs prepared at 800 °C the CH_4 adsorption is severely hindered, leading to a reduced adsorbed amount of CH_4 and consequently to an improved CO_2/CH_4 selectivity of 40. Furthermore, owing to the shrinking pores, the adsorption rates of CH_4 and CO_2 decrease with higher carbonization temperature.

Keywords Biogas upgrading · Separation · CO_2 capture · Carbon molecular sieve · Breakthrough analysis

1 Introduction

Methane (CH_4) is a commonly used energy carrier (as well as a base chemical) and usually obtained from the extraction of natural gas. In order to defossilize the energy supply, CH_4 obtained from biogas is a suitable alternative [1, 2]. However, raw biogas contains various impurities like CO_2, H_2S, H_2, N_2, O_2, NH_3 or Siloxanes with the main impurity being CO_2 [3, 4]. The CO_2 content can range from traces up to 50% with the typical range being 25–50% [4, 5]. In order to use biogas as an energy carrier and feed it to the grid, the CO_2 has to be removed [6, 7]. The separation of CO_2 can be performed by amine scrubbing [3, 8, 9], by membrane processes [8–10] or by adsorption process [8, 9, 11, 12].

In an adsorption process the gas mixture is fed into an adsorber column and the CO_2 is removed from the gas stream by adsorption on a suitable adsorbent, whereas the CH_4 is obtained in pure form at the end of the adsorber column. The regeneration of the adsorbent saturated with CO_2 can be performed by a change of pressure using either pressure swing adsorption (PSA) [13, 14] or vacuum swing adsorption (VSA) [15, 16] or by a change of temperature by purging with a hot gas (temperature swing adsorption, TSA) [17] or heating the adsorbent electrically (electric swing adsorption, ESA) [18–20]. In general, TSA processes are more efficient for the removal of components with a low content due to the comparably long cooldown phase, whereas PSA processes are more efficient for the removal of components with a high content due to the energy needed to pressurize the whole gas phase [21]. A key component in such a process is the adsorbent itself. It should feature a high adsorption capacity for the component(s) to be removed, a high selectivity, a good stability and low costs [22]. Two

✉ Victor Selmert
v.selmert@fz-juelich.de

[1] Institute of Energy and Climate Research: Fundamental Electrochemistry (IEK-9), Forschungszentrum Jülich GmbH, Jülich, Germany

[2] Institute of Physical Chemistry (IPC), RWTH Aachen University, Aachen, Germany

general concepts can be applied to achieve a high selectivity for the separation of the desired components, namely equilibrium or kinetic effects [23]. The first utilizes a difference in the equilibrium loading of the different components. A typical example is the purification of hydrogen that is only adsorbed in low quantities due to its low condensability at room temperature, whereas the other components have much higher adsorption capacities [24, 25]. The kinetic separation makes use of steric effects, leading to a slow adsorption rate and in the limiting case to a size exclusion effect. For example, the separation of O_2 and N_2 in a PSA process utilizes the different sorption rates of both components on a molecular sieve [26]. A similar separation approach is also possible for CO_2 and CH_4 as there is a difference in size of both molecules [27].

In the literature, different adsorbents have been studied for the separation of CH_4 and CO_2, mostly activated carbons (AC) [28, 29], carbon molecular sieves (CMS) [11, 29] and zeolites [29–32]. For example, Grande et al. [28] measured breakthrough curves of 10% and 20% CO_2 in CH_4 on an activated carbon. Silva et al. [31, 32] investigated binary breakthrough curves of CO_2 and CH_4 on zeolite 13X with special regard to the sorption kinetics. Canevesi et al. [11] measured pure gas adsorption data on the carbon molecular sieve KP 407 and simulated its behavior in a 6-step PSA process. Möller et al. [29] compared the separation performance of zeolite 13X, a carbon molecular sieve and an activated carbon and highlighted the suitability of molecular sieves for the CO_2/CH_4 separation over the use of activated carbons.

Recently, electrospun polyacrylonitrile-based (PAN-based) carbon nanofibers (CNFs) were reported that feature smaller pore sizes at higher carbonization temperatures, leading to a tailorable molecular sieve effect [27, 33]. Studies on the sorption kinetics of these CNFs confirmed the molecular sieve effect [34]. In addition, breakthrough experiments with CO_2 and N_2 revealed excellent CO_2/N_2 selectivity [35]. Structural investigations of these CNFs were done using transmission electron microscopy [36, 37] as well as atomic force microscopy [38].

In this work, electrospun PAN-based carbon nanofibers carbonized at various temperatures are evaluated for the separation of CO_2 from CH_4. Pure component isotherms of CH_4 and CO_2 are discussed and based on this data the CO_2/CH_4 selectivity is predicted using the Ideal Adsorbed Solution Theory (IAST). These results are compared to the measured CO_2/CH_4 selectivity obtained from breakthrough experiments with 6% CO_2 and 14% CH_4 in 80% He at 10 bar and 25 °C. For a precise estimation of the adsorbed amount of CH_4 and more detailed insights, desorption curves were recorded as well. In addition, the adsorption kinetics are analyzed by fitting a modeling approach using the linear driving force (LDF) model to the measured data to obtain the adsorption rate constant.

2 Results

2.1 Adsorption isotherms

To investigate the CO_2/CH_4 separation capabilities of PAN-based carbon nanofibers (CNFs), at first, pure component isotherms were measured. Figure 1 depicts isotherms of CH_4 and CO_2 measured at 25 °C on CNFs carbonized at various temperatures ranging from 600 to 900 °C. The CH_4 isotherms (Fig. 1a) of the CNFs prepared in the temperature range from 600 to 750 °C are all similar, as they adsorb 0.56–0.58 mmol g^{-1} of CH_4 at 1.0 bar and feature a slightly concave isotherm shape with regard to the pressure axis. For CNFs prepared at higher temperatures than 750 °C, the isotherm shape changes to almost linear. In addition, the adsorbed amount of CH_4 decreases to 0.34 mmol g^{-1} for CNFs prepared at 800 °C and to 0.01 mmol g^{-1} for CNFs

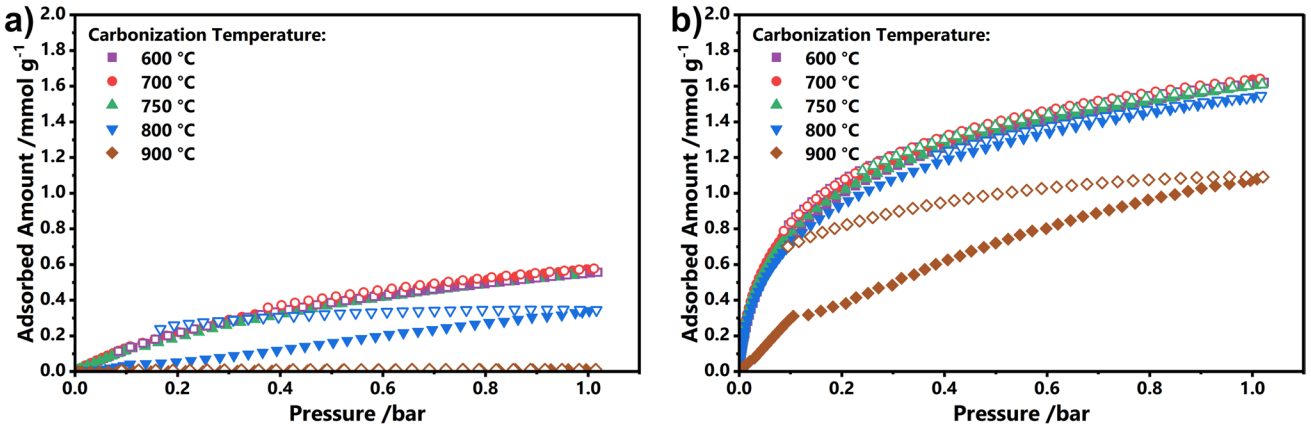

Fig. 1 Isotherms of CH_4 (**a**) and CO_2 (**b**) measured at 298 K on PAN-based carbon nanofiber pellets carbonized at various temperatures ranging from 600 to 900 °C. Closed symbols represent adsorption, open symbols desorption

prepared at 900 °C. In addition, a strong pseudo-irreversibility is observed on the CNFs carbonized at 800 °C, indicating kinetic limitations of the adsorption and desorption process.

A similar observation can be made for the CO_2 isotherms, but in a different carbonization temperature range. Here, the CO_2 isotherms of the CNFs prepared up to 800 °C show almost identical behavior, while a significant decrease in the adsorbed amount of CO_2 as well as a strong pseudo-irreversibility is only visible for the CNFs carbonized at 900 °C. This effect has already been discussed in previous works [27, 33, 35] and is attributed to a size exclusion effect. The CNFs feature a high amount of narrow ultramicropores that shrink when the CNFs are treated with a higher carbonization temperature. Thus, CO_2 and CH_4 can adsorb in the pores CNFs carbonized at 700 °C and below. On elevating the carbonization temperature to 800 °C, CO_2 can still adsorb while CH_4 is excluded by its size. At some point, when the CNFs are carbonized at even higher temperatures, neither CO_2 nor CH_4 can penetrate the pore structure of the material. In comparison to CO_2, the exclusion of CH_4 from the pores takes place on CNFs that were carbonized at a lower temperature (800 °C for CH_4 compared to 900 °C for CO_2), as the CH_4 molecule (critical diameter: 400 pm [39]) is larger than the CO_2 molecule (critical diameter: 280 pm [39]). The pseudo-irreversibility that occurs in the carbonization temperature range of size exclusion can be attributed to the severe diffusion resistance induced by the pores having a similar size as the gas molecule.

A comparison of the CH_4 and CO_2 isotherms reveals that even on CNFs prepared below 800 °C where pores are accessible for both, CO_2 and CH_4, CO_2 is adsorbed in higher quantities (about 1.6 mmol g^{-1} CO_2 vs. 0.56 mmol g^{-1} CH_4 at 1.0 bar on CNFs prepared at 600 °C) indicating a higher affinity of the CNFs to CO_2. This observation is found in literature for different materials [11, 28, 29, 31] and can be attributed to several effects: the interaction with the adsorbent as induced by the surface chemistry (CO_2 can act as Lewis acid and interact with nitrogen moieties, whereas CH_4 cannot), the higher condensability of CO_2 compared to CH_4 and the fact that the same pore volume can accommodate more CO_2 molecules than larger CH_4 molecules.

For CNFs carbonized at 800 °C the adsorbed amount of CH_4 is reduced due to the size exclusion effect, while the adsorbed amount of CO_2 is still high. Consequently, the isotherms suggest an even better separation on these CNFs. For CNFs carbonized at 900 °C and above, a reduction in the CO_2 capacity takes place, making the CNFs less suitable for the adsorption of CO_2.

2.2 Kinetics of the breakthrough experiments

For detailed insights into the CO_2/CH_4 separation on the CNFs, breakthrough experiments were conducted with a gas mixture consisting of 6% CO_2, 14% CH_4 and 80% He at 25 °C and 10 bar total pressure. Besides the breakthrough curves that are shown in Fig. 2, desorption curves of CH_4 and CO_2 were measured following the breakthrough by purging with He at 10 bar after saturation of each component was reached. The complete breakthrough experiments as well as the desorption curves can be found in the Supporting Information (Figs. S1, S2). In the following, the breakthrough curves and their kinetics are discussed qualitatively as well as quantitatively. Afterwards, the amount of adsorbed and desorbed CH_4 and CO_2 is evaluated and the adsorption selectivity of CO_2 over CH_4 is derived.

The measured breakthrough curves of CH_4 and CO_2 (solid lines) on CNFs carbonized in the temperature range from 600 to 900 °C are shown in Fig. 2 together with the curves of the modeling approach (dashed lines), which will be discussed later. In addition, breakthrough curves for CH_4 and CO_2 of a blank run are displayed (dotted lines). As discussed in the Sect. 2.3, the blank run accounts for contributions of the void volume and thus, the amount of adsorbed gas corresponds to the area between the blank and the sample run.

In general, the breakthrough of CH_4 occurs much earlier than the breakthrough of CO_2, e.g., the time at which $c/c_0 = 0.5$ ($t_{0.5}$) is 326 s for CH_4 and equals 1050 s for CO_2 on the CNFs prepared at 600 °C. The difference in breakthrough period is expected due to the lower adsorption capacity of CH_4 compared to CO_2 (Fig. 1) and the higher CH_4 content in the gas phase, leading to a faster saturation with CH_4. The difference in breakthrough times result in a so-called roll-up effect, in which the normalized concentration of CH_4 at the outlet rises above 1.0 due to the absence of CO_2 and a displacement of already adsorbed CH_4 by CO_2. A roll-up of CH_4 is observed for the CNFs carbonized in the range from 600 to 800 °C (Fig. 2a–d).

An assessment of the shape of the breakthrough curves reveals insights about the adsorption kinetics. In general, for type I isotherms under equilibrium conditions, the shape of a breakthrough curve should be steep and focused [40]. However, a breakthrough curve will flatten and spread out more as the system becomes more kinetically limited. In direct comparison all samples exhibit significant differences in the CH_4 breakthrough behavior, as they feature different shapes and breakthrough durations. For a clear illustration, Fig. 3 shows a bar diagram highlighting the onset of the CH_4 breakthrough (lower end), the time at $c/c_0 = 0.5$ ($t_{0.5}$, central line) and $c/c_0 = 1.0$ (upper end). $t_{0.5}$ can be seen as a rough estimation of the adsorbed amount. The height of a bar is a measure for the dispersion of a breakthrough curve. On the CNFs prepared at 600 °C (Fig. 2a) both, CH_4 and CO_2, exhibit steep and focused curves. However, on the CNFs prepared at 700 °C, the breakthrough curve of CH_4 is more disperse (Fig. 2b) and hence, displays a significant higher bar in

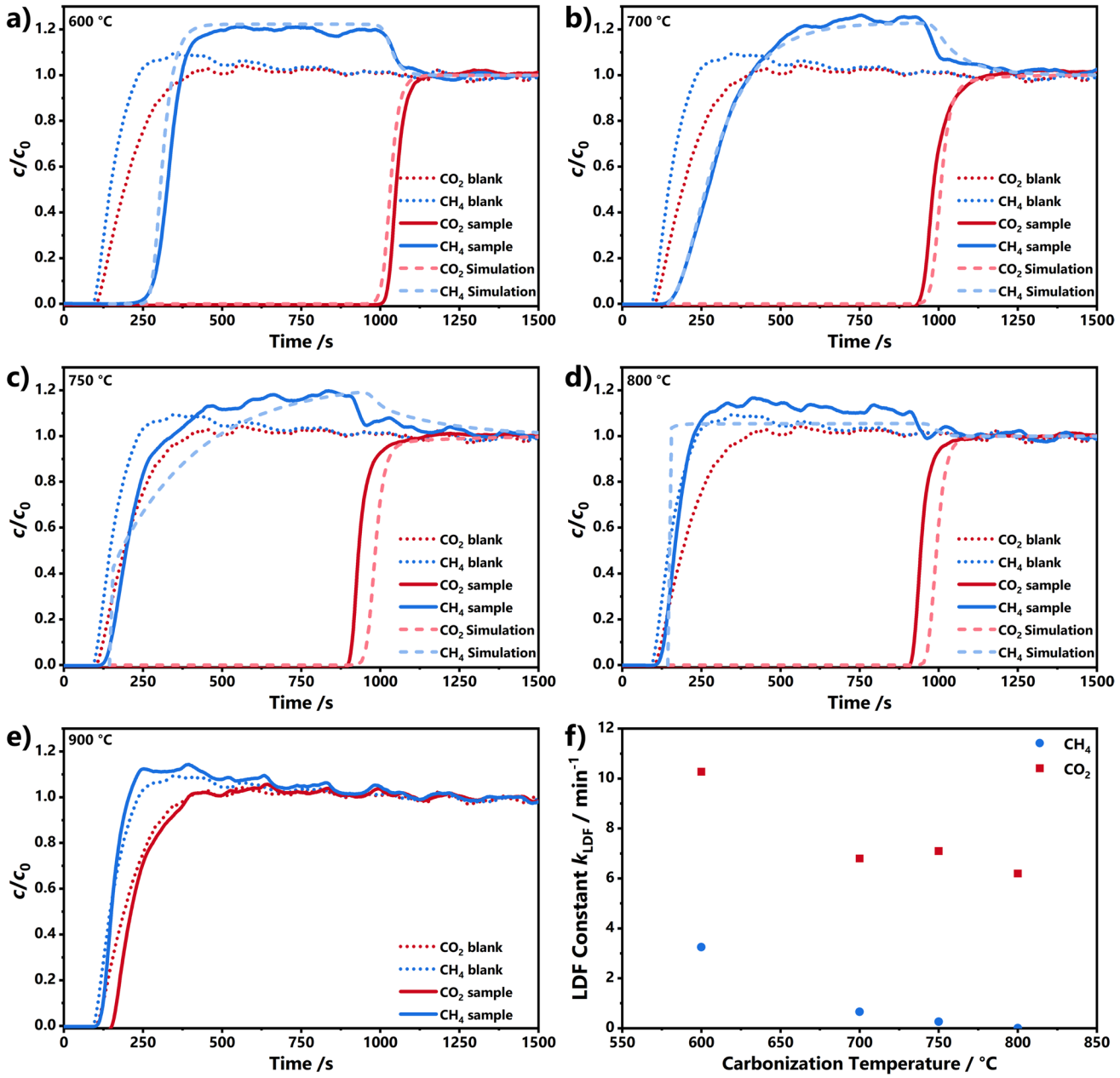

Fig. 2 Breakthrough curves of CO_2 und CH_4 measured on PAN-based carbon nanofiber pellets carbonized at 600 °C (**a**), 700 °C (**b**), 750 °C (**c**), 800 °C (**d**) and 900 °C (**e**) as well as the adsorption rate constant obtained from the modeling of the breakthrough curves (**f**). Both, blank (dotted lines) and sample measurement (solid line), were acquired at 298 K and 10 bar with a gas composition of 6% CO_2, 14% CH_4 and 80% He and a flowrate of 50 ml min^{-1}. The dashed lines represent the results from the modeling approach

Fig. 3. In addition, the onset of the CH_4 breakthrough starts earlier at already at 135 s compared to 230 s for the CNFs carbonized at 600 °C. A similar observation can be made for the CH_4 breakthrough curve on the CNFs prepared at 750 °C that features a flat curve as well (Fig. 2c). A comparison of the average breakthrough time at $c/c_0 = 0.5$ shows a continuous decrease from 326 s for CNFs prepared at 600 °C to 164 s for CNFs prepared at 800 °C (Fig. 3), indicating a decrease in the adsorbed amount of CH_4. The same is visible in Fig. 2a–d as the area between the blank and the sample curve is reduced for CNFs prepared at higher carbonization temperatures. This trend intensifies on the CNFs carbonized at 800 °C, where the area between sample and blank run shrinks in such a way that the CH_4 breakthrough curve almost resembles the curve of the blank run (Fig. 2d). A similar observation can be made for the CH_4 breakthrough on the CNFs carbonized at 900 °C (Fig. 2e).

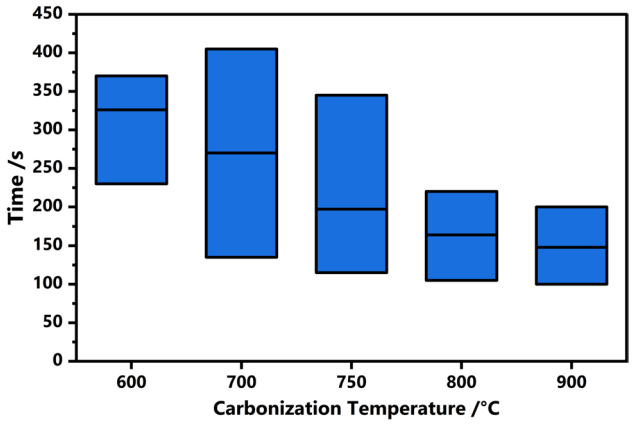

Fig. 3 Characteristic times of the CH_4 breakthrough curves. The lower end of a bar represents the onset of the CH_4 breakthrough, whereas the upper end of a bar represents complete breakthrough ($c/c_0 = 1.0$). The central line highlights the time at which $c/c_0 = 0.5$. The values are listed in Table S1 as well

Up to a carbonization temperature of 800 °C, the breakthrough curves of CO_2 show only minor differences as these samples feature a long breakthrough period for CO_2 with steep breakthrough curves. However, on the CNFs carbonized at 900 °C, the breakthrough period is significantly shorter as the breakthrough of CO_2 starts already at 150 s. As a result, the sample run of CO_2 almost resembles the blank run, which was observed for CH_4 as well, indicating that neither CH_4 nor CO_2 is adsorbed in significant amounts.

The change of the shape of the CH_4 breakthrough curves on the different samples is an interesting observation, since it reveals important insight into the adsorption kinetics. The concave CH_4 isotherms up to CNFs carbonized at 750 °C (Fig. 1a) should lead to focused breakthrough curves. However, for CH_4 this is only observed for CNFs carbonized at 600 °C. On CNFs prepared at 700 and 750 °C the breakthrough curves of CH_4 are disperse, indicating an insufficient adsorption rate to obtain the thermodynamically favored shape. Furthermore, the adsorption capacity on the latter sample seems to be reduced due to the slow adsorption rate, as the area between blank and sample run decreased (although CH_4 as well as CO_2 feature similar isotherms on the CNFs carbonized at 700 and 750 °C). These observations indicate a continuous decrease in the adsorption rates of CH_4 from CNFs prepared at 600 °C to CNFs prepared at 800 °C.

To gain in-depth insights into the adsorption kinetics, the breakthrough processes were modeled with the linear driving force approach (LDF) [41] using the commercial software 3PSim. According to this approach the adsorption rate is proportional to the difference in equilibrium loading $q_{\mathrm{eq},i}$ and current loading q_i for the corresponding component i:

$$\frac{\partial q_i}{\partial t} = k_i\left(q_{\mathrm{eq},i} - q_i\right) \tag{1}$$

The constant k_i is a measure for the rate of adsorption for the component i and was obtained by fitting the rate constant of CO_2 and CH_4 to the corresponding breakthrough data. For the simulation the following assumptions were made:

- The LDF model can sufficiently describe the adsorption process.
- The gas phase can be described with the ideal gas law.
- Based on the low amount of adsorbent (1.5 g) isothermal conditions were assumed.
- The radial dispersion can be neglected.
- The axial dispersion can be described as dispersed plug flow.
- The pressure drop along the column is negligible.
- The column is homogenously packed.

The isotherm data of CH_4 and CO_2 from Fig. 1 was implemented into the simulation by a dual site Langmuir Sips isotherm model:

$$q_{\mathrm{eq}} = \frac{q_{\max}}{2}\left[\frac{K_1\,p}{1+K_1\,p} + \frac{\left(K_2\,p\right)^b}{1+\left(K_2\,p\right)^b}\right] \tag{2}$$

q_{eq} represents the equilibrium loading, $q_{\max}$ the maximal loading, K_1 and K_2 the affinity constants, p the pressure and b the heterogeneity exponent. $q_{\max}$, b, K_1 and K_2 are fit parameters. The fit of the isotherms as well as the fit parameters are given in Fig. S3 and Tables S2 and S3 in the Supporting Information. Further parameters for the simulation are given in Table S4. To account for the competitive adsorption of CH_4 and CO_2, the amount adsorbed was predicted by the Ideal Adsorbed Solution Theory (IAST) by Myers and Prausnitz [42]. A detailed description of the implemented formulas can be found in the Supporting Information.

The modeling of the breakthrough experiment supports the finding of a slower adsorption with higher carbonization temperature, as the obtained adsorption rate for CH_4 and CO_2 both decrease with increasing carbonization temperature (Fig. 2f). For CO_2, the decrease is moderate, changing from 10.2 min^{-1} for the CNFs carbonized at 600 °C to 6.2 min^{-1} for the CNFs carbonized at 800 °C. However, for CH_4 a significant decrease from 3.3 min^{-1} for the CNFs prepared at 600 °C to 0.66 min^{-1} for CNFs prepared at 700 °C and a further decrease to 0.26 min^{-1} on the CNFs carbonized at 750 °C is observable. For the CNFs carbonized at 800 °C, the value is significantly lower. It should be noted that the adsorption rate constant of the CNFs carbonized at 800 °C is only a rough estimation of the order of magnitude, because no meaningful fit to the CH_4 breakthrough curve could be performed, as the curve mostly resembles the blank run (and

the simulation was performed under the assumption of an ideal concentration step). Therefore, the order of magnitude for the adsorption rate constant was estimated at which an immediate breakthrough of CH_4 occurs. Here a value of 0.001 min^{-1} was used. No simulation was performed on the data of the CNFs prepared at 900 °C, as CO_2 as well as CH_4 resemble the curves of the blank run and thus, no meaningful fitting could be performed. Nonetheless, the modeling approach clearly underlines the severe kinetic limitations of the CH_4 adsorption with increasing carbonization temperature, since the adsorption rate constant of CH_4 declines by multiple orders of magnitude from the CNFs prepared at 600 °C to the CNFs prepared at 800 °C (Fig. 2f).

These observations can be attributed to the shrinkage of the ultramicropores on the CNFs with increasing carbonization temperature. The smaller pores increase the diffusion resistance and thus, reduce the adsorption rate constant on CNFs carbonized at higher temperature and lead to a flattening of the CH_4 breakthrough curves on CNFs prepared at 700 and 750 °C. Ultimately, the reduction in the adsorption rate results in a decreased apparent adsorption capacity for the CNFs carbonized at 750 °C. On the CNFs carbonized at 800 and 900 °C, at the point where size exclusion takes place, an almost immediate breakthrough of CH_4 is observed. For CO_2 the size exclusion is observable as well, comparing the CNFs carbonized at 800 and 900 °C, since the breakthrough of CO_2 occurs significantly earlier on the CNFs prepared at 900 °C as on the CNFs prepared at 800 °C.

2.3 CO_2/CH_4 selectivity

When evaluating the separation capabilities of a material, the selectivity can be used as a performance indicator to compare different materials. The CO_2/CH_4 selectivity can be calculated according to Eq. 3:

$$S_{CO_2/CH_4} = \frac{q_{CO_2}}{q_{CH_4}} \frac{y_{CH_4}}{y_{CO_2}} \tag{3}$$

q_i denotes the amount of adsorbed i and y_i denotes the volume fraction of i in the gas phase. The fraction in the gas phase of each component is given by the chosen conditions of the breakthrough experiment, while the amount of adsorbed CO_2 and CH_4 (q_i) can be obtained by integration of the breakthrough curves. For an accurate assessment of the adsorbed amount, especially if only low amounts of gas are adsorbed, it is necessary to accurately quantify the contributions of the void volume. Thus, a procedure is applied, which was described previously [35] and is additionally depicted in Fig. S4 in the Supporting Information. Here, the contributions of the void volume are measured by a blank run with glass beads as inert filling material under the same conditions as the sample run. Consequently, an integration of the blank run yields a value for the void volume, while an integration of the sample run yields a value that consists of contributions of the void volume and contributions of the adsorption. Hence, the amount of adsorbed gas $q_{ads,i}$ is obtained by subtracting the blank value $q_{blank,i}$ from the sample value $q_{sample,i}$:

$$q_{ads,i} = q_{sample,i} - q_{blank,i} \tag{4}$$

The adsorbed amounts of CH_4 and CO_2 for the different samples obtained from the breakthrough experiments are shown in Fig. 4a. It has to be noted that on most samples the breakthrough of CH_4 occurs early (600 °C: $t_{0.5} = 326$ s) compared to CO_2 (600 °C: $t_{0.5} = 1050$ s) leading to a roll-up of CH_4 over a long period of time (600 °C: 720 s). During that time adsorbed CH_4 might be displaced by CO_2 and eluted over a long period of time, resulting in only a small change in concentration and, thus, making a precise quantification of the light component (CH_4) challenging as reported in literature [35, 43–45]. The adsorption values of CH_4 were obtained from an integration up to the CH_4 roll-up, but do not include the roll-up, since including the roll-up led to negative CH_4 loadings for some samples. Consequently, displaced CH_4 during the roll-up is not considered in the adsorption values, which for some samples might lead to an overestimation of adsorbed CH_4.

Wilkins et al. [43, 45] proposed to measure desorption curves by purging with the carrier gas and use these curves for a more precise quantification of the adsorbed amount of the light component (here CH_4). Thus, in addition to the values obtained from the breakthrough curves, values from the integration of the desorption curves are shown as well.

In general, the adsorbed amount of gas in Fig. 4a is higher for CO_2 than for CH_4, indicating a higher affinity to CO_2 than CH_4. In the adsorption branch of CO_2, a slight decrease is observable from CNFs prepared at 600 °C (1.29 mmol g^{-1}) to CNFs prepared at 800 °C (1.14 mmol g^{-1}) followed by a significant reduction in capacity to CNFs carbonized at 900 °C (< 0.1 mmol g^{-1}). For CH_4 similar observations can be made but shifted to lower carbonization temperatures. On CNFs carbonized at 600 and 700 °C the CH_4 capacity is rather high (0.5–0.6 mmol g^{-1}) and then declines significantly on the CNFs carbonized at 800 °C (< 0.1 mmol g^{-1}). The severe reduction of the adsorption capacity is attributed to the size exclusion effect, taking place for CO_2 in the range from 800 to 900 °C and for CH_4 from 700 to 800 °C. Due to the shift in carbonization temperature for the size exclusion, the CNFs prepared at 800 °C are highlighted as a suitable separation material, as CO_2 is adsorbed in high quantities but CH_4 not.

A comparison of the results obtained from the integration of the breakthrough curves and the desorption curves,

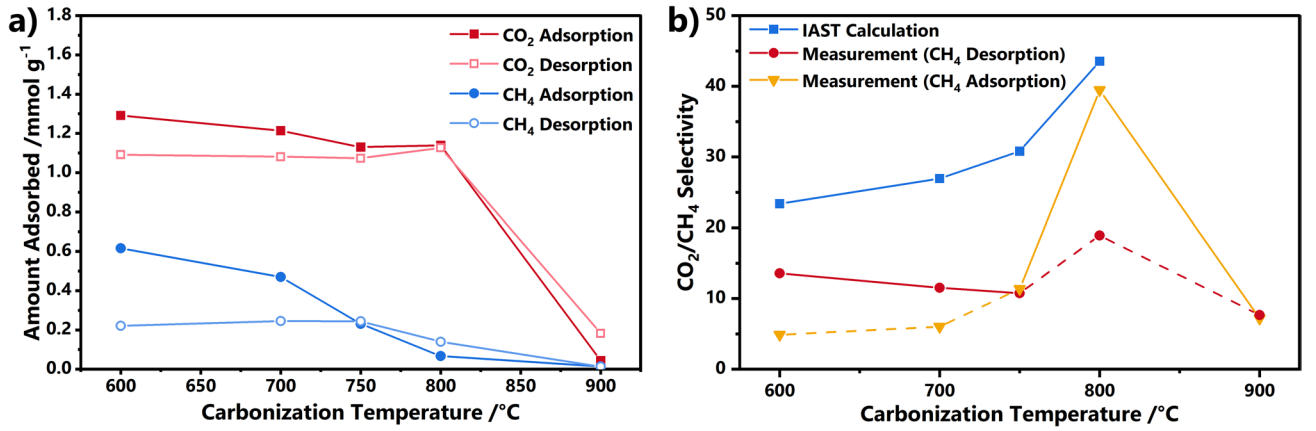

Fig. 4 **a** Adsorbed amount of CO_2 and CH_4 quantified by integration of the breakthrough experiments shown in Fig. 2 (Adsorption) and the desorption curves in Fig. S2 (Desorption). **b** CO_2/CH_4 selectivity calculated according to Eq. 3 from the breakthrough data and IAST calculations at 25 °C and 2 bar and a CO_2/CH_4 ratio of 30/70. In order to calculate the measured CO_2/CH_4 selectivity (Eq. 3), for the loading of CO_2, the adsorption value was used, whereas for the loading of CH_4 the desorption value (red circle) or the adsorption value (orange triangle) was used. The more representative values are connected with a solid line, the values regarded as less precise are connected with a dashed line. For the IAST calculations the CO_2 and CH_4 isotherms in Fig. 1 were fitted with a dual site Langmuir Sips isotherm model (Eq. 2). The parameters of the fit are shown in Tables S2 and S3 in the SI (Color figure online)

reveals deviations for most of the CNFs. For CO_2 the desorption values are below the adsorption values in the carbonization temperature range from 600 °C (0.2 mmol g^{-1}) to 750 °C (0.06 mmol g^{-1}), then match for 800 °C and finally are higher on CNFs prepared at 900 °C. The first observation can be attributed to the dispersive nature of the CO_2 desorption curves (Fig. S2), resulting from the concave shape of the CO_2 isotherm on these CNFs [40]. Consequently, the desorption of CO_2 is stretched over a long period of time with the result that complete desorption was not observed in the time frame of the experiment. With increasing carbonization temperature, the desorption curves become slightly less dispersive, as depicted in Fig. S2. As a consequence, the difference between adsorption and desorption value decreases for higher carbonized CNFs and results finally in a matching capacity for the 800 °C fibers. For the CNFs carbonized at 900 °C, the desorption capacity is above the adsorption capacity leading seemingly to a contradiction, which has been reported for CO_2 breakthrough experiments on the CNFs carbonized at 900 °C before [35]. As discussed in the isotherms and kinetics sections, the CO_2 adsorption of the CNFs carbonized at 900 °C is limited by severe kinetic restrictions. As shown in Fig. 2e, the adsorption period of CO_2 is very short until the CO_2 breakthrough is observed, resulting in a low amount of adsorbed CO_2 (0.04 mmol g^{-1}), which is significantly below the loading of the corresponding CO_2 isotherm (0.7 mmol g^{-1}) at these conditions. After the breakthrough, the gas phase composition was kept constant for 20 min before the desorption curves were measured. During this period, additional CO_2 could adsorb and consequently, desorb during the desorption experiment. However, the adsorption rate after the breakthrough is too low to distinguish removed CO_2 due to adsorption from signal fluctuations, making a quantification of the CO_2 adsorbed after the breakthrough not feasible. Since the desorption curve could be integrated over a considerably longer time frame than the breakthrough measurement (2 h for the desorption vs. 5–6 min for adsorption) and does not contain signal fluctuations from the mass flow controllers, more time for equilibration was given and thus, more CO_2 could be quantified during the desorption experiment.

For CH_4 a much higher adsorption capacity than desorption capacity is found on CNFs prepared at 600 or 700 °C. Matching adsorption and desorption values are found on CNFs prepared at 750 °C as well as 900 °C. For the CNFs prepared at 800 °C, a higher desorption value than adsorption value is observed. The deviations on the CNFs prepared at low temperatures stem from neglecting the roll-up in the integration of the breakthrough curves and thus, neglecting a displacement of CH_4 by CO_2. The desorption curves include these contributions and thus, are representative of the actual adsorbed amount of CH_4. The CNFs prepared at 800 °C feature the same effect for CH_4 as discussed for CO_2 on the CNFs prepared at 900 °C. The adsorbed amount of CH_4 does not reach equilibrium as severe kinetic limitations are present leading to further adsorption after the breakthrough as the composition was kept constant for 40 min. The integration of the desorption was performed over a longer period of time compared to the adsorption, resulting in a better equilibration and, thus, a higher quantified amount of adsorbed CH_4 from the desorption curve. On the CNFs carbonized at 750 °C the adsorption and desorption values match, as the two opposing effects, under-equilibration due to kinetic

Table 1 Values for the CO_2/CH_4 selectivity on different materials reported in literature and measured with binary CO_2/CH_4 breakthrough experiments

Sample	CO_2/CH_4 selectivity	Temperature/K	Sum of CO_2+CH_4 pressure/bar	Composition CO_2/CH_4	References
600 °C CNFs	13.6	298	2	30/70	This work
700 °C CNFs	11.5	298	2	30/70	This work
750 °C CNFs	10.8	298	2	30/70	This work
800 °C CNFs	39.5	298	2	30/70	This work
900 °C CNFs	7.7	298	2	30/70	This work
Zeolite 13X	36.3	313	0.65	25/75	[32]
Zeolite 13X	19.7	313	1.96	25/75	[32]
Zeolite 13X	14.4	313	3.27	25/75	[32]
Zeolite 13X	10.8	423	1.96	25/75	[32]
Zeolite 13X	7.1	479	1.96	25/75	[32]
Maxsorb (AC)	3.1[a]	298	5	10/90	[28]
Maxsorb (AC)	3.3[a]	298	25	10/90	[28]
Maxsorb (AC)	2.5[a]	298	50	10/90	[28]
Maxsorb (AC)	3.4[a]	298	5	20/80	[28]
Maxsorb (AC)	3.4[a]	298	25	20/80	[28]
Maxsorb (AC)	3.0[a]	298	50	20/80	[28]
CPDA@A-Cs (carbon composite)	5.1	298	1.00	50/50	[47]
Cu-BTC	6.5[b]	303	1.1[b]	25/75	[48]
Cu-BTC	5.6[b]	303	1.1[b]	50/50	[48]
Cu-BTC	6.6[b]	303	1.1[b]	75/25	[48]
Shirasagi MSC CT-350	15.08	303	1.0	40/60	[49]
Shirasagi MSC CT-350	26.32	303	1.0	10/90	[49]
Organosorb 10-CO	2.89	303	1.0	40/60	[49]
CMS-240	12.71	303	1.0	40/60	[49]
CMS-240	34.74	303	1.0	10/90	[49]
CMS KP407[a,b,c]	14.9	314.65	10	10/90	[50]

[a]Selectivity calculated according to Eq. 3 from the reported breakthrough data

[b]Values were read from diagram

[c]Estimated at an axial position of 0.1 m at $t = 2000$ s

restrictions and overestimation of the adsorbed amount due to neglecting the roll-up, counterbalance each other.

In conclusion, for CO_2 the adsorption branch represents the more reliable value for the adsorbed amount as the desorption slightly underestimates the adsorbed amount of CO_2 due to the dispersive desorption curves and the limited time frame of the experiment.

CH_4 is more accurately quantified by the desorption curves for CNFs prepared up to 750 °C, as both CH_4 adsorption and CH_4 displacement by CO_2 is considered in this method. For the CNFs carbonized at 800 °C the CH_4 adsorption is governed by the slow adsorption kinetics leading to a correlation of the duration of adsorption and the quantified amount of CH_4. Because the time the composition was kept constant until desorption was measured (40 min) was considerably longer than the breakthrough experiment, it is assumed that most of the additionally adsorbed CH_4 quantified by the desorption curve, is adsorbed after complete CO_2 breakthrough occurred. Therefore, the adsorption value is considered the more realistic for CH_4 on this sample.

In consideration of this, the amount of adsorbed CO_2 on the CNFs carbonized up to 800 °C is in the range of 1.14–1.29 mmol g^{-1}, which is slightly below the pure CO_2 capacity of 1.25–1.35 mmol g^{-1} from Fig. 1. The amount of adsorbed CH_4 stays almost constant for CNFs carbonized in the range from 600 to 750 °C (0.22–0.24 mmol g^{-1} at a partial pressure of 1.4 bar), which is significantly lower than the pure CH_4 uptake at 1 bar shown in Fig. 1 (0.55–58 mmol g^{-1}). These deviations from the pure component adsorption isotherms indicate a strong displacement of CH_4 by CO_2, which is indicative of strong competitive mixed gas adsorption equilibria. CNFs prepared at 800 °C feature a smaller CH_4 loading of 0.07 mmol g^{-1} indicating an even better separation on this sample. For deeper insights into

the separation capabilities of the CNFs, the CO_2/CH_4 selectivity was calculated according to Eq. 3 and is displayed in Fig. 4b. For the calculation the adsorption value of CO_2 was used, while for CH_4 the adsorption (red circle) as well as the desorption value (orange triangle) were used. The results are shown together with values predicted by the Ideal Adsorbed Solution Theory (IAST) [42] based on the dual site Langmuir Sips fits to the isotherms in Fig. 1 (Fig. S3). The measured CO_2/CH_4 selectivity stays rather constant for the CNFs carbonized in the range from 600 to 750 °C with values of 10.8 to 13.6 (CH_4 desorption) or 4.9 to 11.4 (CH_4 adsorption) already indicating a rather selective adsorption of CO_2. Even higher values of 18.9 (CH_4 desorption) and 39.5 (CH_4 adsorption) are realized on the CNFs prepared at 800 °C, as the size exclusion of CH_4 appears, highlighting this material as a highly selective adsorbent for CO_2/CH_4 separation. For a carbonization temperature of 900 °C the selectivity drops again to 8, since the size exclusion of CO_2 from the pores takes place on this sample, leading to an extremely small CO_2 capacity and making these CNFs unsuitable as an adsorbent. As discussed above, the CH_4 desorption value is more representative in the range from 600 to 750 °C (selectivity of 10.8 to 13.6), whereas for CNFs prepared at 800 °C the adsorption value of CH_4 is more accurate (selectivity of 39.5).

In comparison, the CO_2/CH_4 selectivity values predicted by the IAST calculations are in general higher (23–44), but show a less significant increase in selectivity from 750 °C (31) to 800 °C (44) as shown in Fig. 4b. The latter can be attributed to the severe kinetic limitations for CH_4 adsorption on the CNFs carbonized at 800 °C. IAST is based on the equilibrium isotherms in Fig. 1, whereas the amount of adsorbed CH_4 on the CNFs carbonized at 800 °C was not governed by equilibrium, but the rate of adsorption. That the IAST calculation resulted in roughly two times higher values in the range from 600 to 750 °C was observed for the CO_2/N_2 selectivity on the CNFs as well [35]. The deviation in the CO_2/CH_4 selectivity is mainly referable to the predicted CH_4 adsorption, which is roughly half as high compared to the measured data (Fig. S5). An explanation for the deviation in CH_4 loading might be that for the less selectively adsorbed component (here CH_4) the spreading pressure is calculated up to a pressure that is higher than the total pressure of the gas phase (here: 2 bar) [42, 46]. Consequently, the isotherm fits of the CH_4 isotherms are extrapolated far beyond the measured pressure range. Therefore, the results of the IAST calculation are dependent on how well the dual site Langmuir Sips model describes the CH_4 isotherm beyond the fitted range.

A comparison of the CO_2/CH_4 selectivity of the CNFs with other materials reported in literature is shown in Table 1. It should be noted that the measurement conditions (pressure, temperature, gas phase composition) reported in other works vary and thus, a direct comparison of these values should be taken with caution. This is especially true, if the separation is based on kinetic limitations and thus, strongly dependent on the conditions of the experiment. The CO_2/CH_4 selectivity reported in literature for carbonaceous materials like the Maxsorb, Organosorb 10-CO or the CPDA@A-Cs is typically in the range of 2–5 under various conditions, which is in agreement with values reported by Peredo-Mancilla et al. [51] for various other carbon materials. The MOF Cu-BTC exhibits a slightly higher selectivity of 5.6–6.6 (30 °C, 1.1 bar) for various CO_2/CH_4 ratios. Compared to this, the CNFs carbonized in the temperature range from 600 to 750 °C show already a good CO_2/CH_4 selectivity with values of 10.8–13.6 (25 °C, 2 bar). The CNFs prepared at 800 °C have an even higher CO_2/CH_4 selectivity of 39.5, as they feature a kinetic separation effect additionally. Their CO_2/CH_4 selectivity is in a similar range as the selectivity of the zeolite 13X (although measured under deviating conditions). Commercial carbon molecular sieves such as the Shirasagi MSC CT-350, the CMS-240 or the CMS KP407 that utilize a kinetic separation effect as well were reported to have a CO_2/CH_4 selectivity in the range from 12.7 to 34.7 depending on the chosen condition [49, 50]. Compared to this, the CNFs prepared at 800 °C feature a similar CO_2/CH_4 selectivity, which highlights these CNFs as a powerful adsorbent for CO_2/CH_4 separation. Moreover, it seems possible to further increase the CO_2/CH_4 selectivity of the CNFs by optimizing the carbonization temperature in the temperature range from 800 to 900 °C. At the optimal carbonization temperature, the diffusion resistance of CH_4 is maximized in order to minimize the CH_4 uptake, while simultaneously the pores are still wide enough to be accessible for CO_2 at a reasonable adsorption rate.

3 Experimental

3.1 Synthesis

All chemicals were used as received without further purification. A solution of 10 wt% polyacrylonitrile (PAN, Homopolymer, 150.000 g mol^{-1}, BOC Science, USA) in *N*,*N*-dimethylformamide (DMF, VWR Chemicals, Germany) was obtained by dissolving 8 g of PAN in 72 g DMF and stirring for 2 days at room temperature. The solution was then processed in an electrospinning device in a climate chamber (IME Technologies, The Netherlands) to produce a PAN-nanofiber mat. As collector a rotating barrel with a length of 18 cm, a diameter of 9.0 cm and a rotating speed of 1000 rpm was used. A nozzle setup consisting of four linear arranged nozzles moved laterally

to the rotating barrel (nozzle-to-nozzle distance: 1.0 cm). The nozzles moved over a distance of 12 cm with a speed of 2.0 cm s^{-1} and a turn delay of 500 ms. The movement was centered on the mid of the collector. The solution was pumped through the nozzles with 30 µl min^{-1} per nozzle (120 µl min^{-1} total). The tip-collector distance equaled 7.5 cm and a voltage of 25 kV was applied. The atmosphere was kept constant at 25 °C with a relative humidity of 30%. After 3 h of electrospinning, a PAN nanofiber mat was obtained.

This fiber mat was stabilized in a drying furnace (Carbolite Gero, Germany) in air at 250 °C for 15 h with a heating rate of 5 K min^{-1}. Afterwards, the fibers were processed into pellets. For this, the stabilized fiber mat was shredded to a fiber powder using a knife mill (IKA A 10 basic, IKA, Germany) with a grinding chamber reduction and a star shaped cutter. The shredding was performed three times for 60 s. After each shredding step the mill was opened and fiber mat fragments sticking to the cap were removed and put back into the grinding chamber. 3 g of the resulting fiber powder was put into a 50 ml beaker together with 5.4 g of a 3.3 wt% solution of PAN (Homopolymer, 150.000 g mol^{-1}, BOC Science, USA) in DMF (VWR Chemicals, Germany) and mixed for several minutes by hand with a spatula to obtain a homogeneous dough-like mass. The dough-like mass was extruded through a 2 mm nozzle onto a petri dish into cylindrical shaped lines. The extrudate was dried at first on a heating plate at 50 °C for 30 min and then in a vacuum drying chamber (Binder, Germany) at 80 °C for at least 1 h. To stabilize the PAN binder of the extrudate, the aforementioned stabilization was carried out again (250 °C, 15 h, 5 k min^{-1}). Afterwards, the extrudate was cut into 2–4 mm long pellets using a scalpel. The nanofiber pellets were carbonized in a tube furnace under an argon atmosphere at various temperatures ranging from 600 to 900 °C. The tube furnace was heated with 5 K min^{-1} and after reaching the desired temperature, it was held for 3 h. Cool down was performed with a rate of 3.3 K min^{-1}.

3.2 Static gas adsorption measurements

CO_2 (4.5, Air Products, Germany) and CH_4 (4.5, Messer, Germany) isotherms were measured with a Quantachrome Autosorb iQ2. The measurement temperature was kept constant at 298 K with a water bath. Prior to each isotherm measurement the samples were outgassed under vacuum at 200 °C for 6 h.

3.3 Breakthrough measurements

Breakthrough curves were measured by 3P Instruments GmbH (Germany) using a mixSorb SHP (3P Instruments GmbH, Germany) with a stainless-steel column (15 cm length, 8 mm inner diameter). A diagram of this device was shown previously [35]. The gas composition at the column outlet was measured with a mass spectrometer (Cirrus 3, MKS, USA). For each sample measurement 1.50 g of CNFs pellets were filled into the column resulting in a filling height of 11.5 cm. Each sample was pretreated at 300 °C for 90 min with a Helium (5.0, Tyczka Industrie-Gase, Germany) flow of 50 ml min^{-1} to remove preabsorbed gases. Afterwards, the column was tempered to 25 °C using a water bath. For each sample the following breakthrough experiment was performed. At 10 bar and 25 °C a mixture of 6 vol% CO_2 (4.5, Tyczka Industrie-Gase, Germany), 14 vol% CH_4 (3.5, Tyczka Industrie-Gase, Germany) and 80 vol% He was flowing through the column with a flowrate of 50 ml min^{-1}. After a complete breakthrough of CO_2 and CH_4 and a steady state was observed, desorption curves were recorded by purging with He. For this the gas mixture was change to 100% Helium at 10 bar and 50 ml min^{-1} for at least 2 h. The complete breakthrough experiment is shown in Fig. S1.

For an accurate integration of the breakthrough curves, a blank run under the same conditions was performed using glass beads with a diameter of 0.4–0.6 mm (VWR, Germany). The amount of glass beads needed to match the void volume of the sample runs was calculated from the density of the glass beads and the average density of the CNFs. The density of the glass beads and the CNFs was measured at 25 °C using a 3P micro 300 (3P Instruments GmbH, Germany). The volume of a sample was determined by the difference of the volume of the measurement cell with sample inside and without sample inside. The volume inside the measurement cell was determined by dosing Helium (6.0, Air Products, Germany). The weight of the sample was measured with a high precision scale (Mettler Toledo, Switzerland). Considering the average density of the CNFs (1.8 g cm^{-3}) and glass beads (2.3 g cm^{-3}), 1.9 g of glass beads were used in the blank run.

Integration of the breakthrough curves was performed using the software mixSorb Manager (Version: 1.4.1.1, 3P Instruments GmbH, Germany). The corresponding equations are shown in the Supporting Information. The breakthrough curves of CO_2 were integrated from the start of the experiment to the time until complete breakthrough was observed. For CH_4 integration of the roll up led partly to unreasonable (negative) loadings, as discussed in the results part. Thus, only the adsorption phase (without the roll-up) from the beginning of the breakthrough experiment to the time when the CH_4 concentration first surpasses the inlet concentration was considered for the integration. The desorption curves of CH_4 and CO_2 were integrated from the start of the desorption up to 120 min.

3.4 Modeling

Modeling of the breakthrough curves was performed with the software 3PSim (Version: 1.1.2.6, 3P Instruments GmbH, Germany). Further details on the implemented formulas can be found in the Supporting Information. For the fit to the experimental data, the dead time of the experimental setup has to be accounted for. Consequently, the time of the blank run until the CH_4 concentration reached half of the input concentration was subtracted from the sample runs.

3.5 IAST calculations

The IAST calculation were performed with the software 3PSim (Version: 1.1.2.6, 3P Instruments GmbH, Germany). The isotherm data was described by dual site Langmuir Sips fits. The fit parameter can be found in Tables S2 and S3 and a visualization of the fit and the measured data is shown in Fig. S3 in the Supporting Information.

4 Conclusion

In this work polyacrylonitrile-based electrospun carbon nanofiber pellets were investigated for the separation of CO_2 and CH_4 using static and dynamic gas adsorption. The pure component isotherms showed a high CO_2 adsorption capacity on CNFs prepared in the temperature range from 600 to 800 °C and a moderate CH_4 adsorption capacity on the CNFs prepared in the temperature range from 600 to 750 °C. On CNFs carbonized at 800 and 900 °C, CH_4 and CO_2, respectively, exhibited a significant decrease in the adsorbed amount and showed severe kinetic limitation visible as pseudo-irreversibility. This was attributed to a shrinkage of the ultramicropores of the CNFs, leading to a size exclusion of CH_4 on the CNFs carbonized at 800 °C and of CO_2 on the CNFs carbonized at 900 °C. Likewise, a slowdown of the adsorption kinetics was observed during the breakthrough experiment performed with a CO_2/CH_4 ratio of 30/70. In the carbonization temperature range from 600 to 800 °C, the decrease in the kinetics for CO_2 was only marginal as the adsorption rate constant of CO_2 obtained from a modeling approach decreased from 10.3 to 6.2 min^{-1}, whereas a more significant decline was present for CH_4. The rate constant of CH_4 decreased from 3.3 min^{-1} on the CNFs prepared at 600 °C to roughly 0.001 min^{-1} on the CNFs prepared at 800 °C, leading to an increase in dispersion of the CH_4 breakthrough curves with higher carbonization temperature. A reduced CH_4 breakthrough period was observed for the CNFs prepared at 750 °C as well as almost immediate breakthrough of CH_4 on CNFs prepared at 800 °C. Consequently, a detailed analysis of the adsorbed amount quantified by adsorption and desorption of CO_2 and CH_4 revealed that due to the kinetic limitations the amount of adsorbed CH_4 significantly decreases on increasing the carbonization temperature from 750 to 800 °C. As a result, good CO_2/CH_4 selectivity values of 10.8–13.6 for the CNFs prepared in the temperature range from 600 to 750 °C are obtained, but on the CNFs carbonized at 800 °C, on which CH_4 adsorption is kinetically hindered, a superior CO_2/CH_4 selectivity of 40 is achieved, highlighting these CNFs as a powerful adsorbent for the separation of CO_2 and CH_4.

Supplementary Information The online version contains supplementary material available at https://doi.org/10.1007/s10450-023-00435-6.

Acknowledgements The authors thank 3P Instruments GmbH for the measurement of the breakthrough data.

Author contributions VS: writing—original draft, visualization, methodology, investigation, conceptualization. AK: writing—review & editing, supervision, investigation, conceptualization. HK: writing—review & editing, supervision, project administration, funding acquisition, conceptualization. HT: writing—review & editing, supervision, project administration, funding acquisition, conceptualization. R-AE: writing—review & editing, supervision, project administration, funding acquisition, conceptualization.

Funding Open Access funding enabled and organized by Projekt DEAL. Funding provided by the Deutsche Forschungsgemeinschaft (DFG, German Research Foundation) under Germany's Excellence Strategy – Cluster of Excellence 2186 "The Fuel Science Center" – ID: 390919832.

Data availability The data that support the findings of this study are available from the corresponding author upon reasonable request.

Declarations

Competing interests The authors have patent #WO2020249441A1 issued to Forschungszentrum Jülich as well as a pending patent application (102023201375.4).

Ethical approval Not applicable.

References

1 Abanades, S., Abbaspour, H., Ahmadi, A., Das, B., Ehyaei, M.A., Esmaeilion, F., El Haj Assad, M., Hajilounezhad, T., Jamali, D.H., Hmida, A., Ozgoli, H.A., Safari, S., AlShabi, M., Bani-Hani, E.H.: A critical review of biogas production and usage with legislations

framework across the globe. Int. J. Environ. Sci. Technol. **19**(4), 3377–3400 (2022). https://doi.org/10.1007/s13762-021-03301-6
2 Mertins, A., Wawer, T.: How to use biogas? A systematic review of biogas utilization pathways and business models. Bioresour. Bioprocess. **9**(1), 1–18 (2022). https://doi.org/10.1186/s40643-022-00545-z
3 Capra, F., Fettarappa, F., Magli, F., Gatti, M., Martelli, E.: Biogas upgrading by amine scrubbing: solvent comparison between MDEA and MDEA/MEA blend. Energy Procedia **148**, 970–977 (2018). https://doi.org/10.1016/j.egypro.2018.08.065
4 Huertas, J.I., Giraldo, N., Izquierdo, S.: Removal of H_2S and CO_2 from biogas by amine absorption. In: Marko, J. (ed.) Mass Transfer in Chemical Engineering Processes, pp. 133–150. IntechOpen, Rijeka (2011)
5 Li, Y., Alaimo, C.P., Kim, M., Kado, N.Y., Peppers, J., Xue, J., Wan, C., Green, P.G., Zhang, R., Jenkins, B.M., Vogel, C.F.A., Wuertz, S., Young, T.M., Kleeman, M.J.: Composition and toxicity of biogas produced from different feedstocks in California. Environ. Sci. Technol. **53**(19), 11569–11579 (2019). https://doi.org/10.1021/acs.est.9b03003
6 Miltner, M., Makaruk, A., Harasek, M.: Application of gas permeation for biogas upgrade—operational experiences of feeding biomethane into the Austrian gas grid. In: Proceedings of the 16th European Biomass Conference & Exhibition, pp. 1905–1911 (2008)
7 Miltner, M., Makaruk, A., Harasek, M.: Review on available biogas upgrading technologies and innovations towards advanced solutions. J Clean. Prod. **161**, 1329–1337 (2017). https://doi.org/10.1016/j.jclepro.2017.06.045
8 Angelidaki, I., Xie, L., Luo, G., Zhang, Y., Oechsner, H., Lemmer, A., Munoz, R., Kougias, P.G.: Biogas upgrading: current and emerging technologies. In: Pandey, A., Larroche, C., Dussap, C.-G., Gnansounou, E., Khanal, S.K., Ricke, S. (eds.) Biomass, Biofuels, Biochemicals, Biofuels: Alternative Feedstocks and Conversion Processes for the Production of Liquid and Gaseous Biofuels, 2nd edn., pp. 817–843. Academic Press, London (2019)
9 Awe, O.W., Zhao, Y., Nzihou, A., Minh, D.P., Lyczko, N.: A review of biogas utilisation, purification and upgrading technologies. Waste Biomass Valoriz. **8**(2), 267–283 (2017). https://doi.org/10.1007/s12649-016-9826-4
10 Chen, X.Y., Vinh-Thang, H., Ramirez, A.A., Rodrigue, D., Kaliaguine, S.: Membrane gas separation technologies for biogas upgrading. RSC Adv. **5**(31), 24399–24448 (2015). https://doi.org/10.1039/C5RA00666J
11 Canevesi, R.L.S., Andreassen, K.A., Da Silva, E.A., Borba, C.E., Grande, C.A.: Pressure swing adsorption for biogas upgrading with carbon molecular sieve. Ind. Eng. Chem. Res. **57**(23), 8057–8067 (2018). https://doi.org/10.1021/acs.iecr.8b00996
12 Grande, C.A.: Biogas upgrading by pressure swing adsorption. In: Dos, S., Bernardes, M.A. (eds.) Biofuel's Engineering Process Technology, pp. 65–84. IntechOpen, Rijeka (2011)
13 Grande, C.A.: Advances in pressure swing adsorption for gas separation. ISRN Chem. Eng. **2012**(9), 1–13 (2012). https://doi.org/10.5402/2012/982934
14 Kacem, M., Pellerano, M., Delebarre, A.: Pressure swing adsorption for CO_2/N_2 and CO_2/CH_4 separation: comparison between activated carbons and zeolites performances. Fuel Process. Technol. **138**, 271–283 (2015). https://doi.org/10.1016/j.fuproc.2015.04.032
15 Arya, A., Divekar, S., Rawat, R., Gupta, P., Garg, M.O., Dasgupta, S., Nanoti, A., Singh, R., Xiao, P., Webley, P.A.: Upgrading biogas at low pressure by vacuum swing adsorption. Ind. Eng. Chem. Res. **54**(1), 404–413 (2015). https://doi.org/10.1021/ie503243f
16 Grande, C.A., Rodrigues, A.E.: Biogas to fuel by vacuum pressure swing adsorption I. Behavior of equilibrium and kinetic-based adsorbents. Ind. Eng. Chem. Res. **46**, 4595–4605 (2007). https://doi.org/10.1021/ie061341
17 Ntiamoah, A., Ling, J., Xiao, P., Webley, P.A., Zhai, Y.: CO_2 capture by temperature swing adsorption: use of hot CO_2-rich gas for regeneration. Ind. Eng. Chem. Res. **55**(3), 703–713 (2016). https://doi.org/10.1021/acs.iecr.5b01384
18 Keller, L., Lohaus, T., Abduly, L., Hadler, G., Wessling, M.: Electrical swing adsorption on functionalized hollow fibers. Chem. Eng. J. **371**, 107–117 (2019). https://doi.org/10.1016/j.cej.2019.04.029
19 Moon, S.-H., Shim, J.-W.: A novel process for CO_2/CH_4 gas separation on activated carbon fibers—electric swing adsorption. J. Colloid Interface Sci. **298**(2), 523–528 (2006). https://doi.org/10.1016/j.jcis.2005.12.052
20 Ribeiro, R.P.P.L., Grande, C.A., Rodrigues, A.E.: Electric swing adsorption for gas separation and purification: a review. Sep. Sci. Technol. **49**(13), 1985–2002 (2014). https://doi.org/10.1080/01496395.2014.915854
21 Lively, R.P., Realff, M.J.: On thermodynamic separation efficiency: adsorption processes. AIChE J. **62**(10), 3699–3705 (2016). https://doi.org/10.1002/aic.15269
22 Oschatz, M., Antonietti, M.: A search for selectivity to enable CO_2 capture with porous adsorbents. Energy Environ. Sci. **11**(1), 57–70 (2018). https://doi.org/10.1039/C7EE02110K
23 Yang, R.T.: Gas Separation by Adsorption Processes, 1st edn. Butterworths, Boston (1987)
24 Luberti, M., Ahn, H.: Review of polybed pressure swing adsorption for hydrogen purification. Int. J. Hydrogen Energy **47**(20), 10911–10933 (2022). https://doi.org/10.1016/j.ijhydene.2022.01.147
25 Sircar, S., Golden, T.C.: Purification of hydrogen by pressure swing adsorption. Sep. Sci. Technol. **35**(5), 667–687 (2000). https://doi.org/10.1081/SS-100100183
26 Ruthven, D.M., Farooq, S.: Air separation by pressure swing adsorption. Gas Sep. Purif. **4**(3), 141–148 (1990). https://doi.org/10.1016/0950-4214(90)80016-E
27 Kretzschmar, A., Selmert, V., Kungl, H., Tempel, H., Eichel, R.-A.: Application of a tailorable carbon molecular sieve to evaluate concepts for the molecular dimensions of gases. Microporous Mesoporous Mater. **343**, 112156 (2022). https://doi.org/10.1016/j.micromeso.2022.112156
28 Grande, C.A., Blom, R., Möller, A., Möllmer, J.: High-pressure separation of CH_4/CO_2 using activated carbon. Chem. Eng. Sci. **89**, 10–20 (2013). https://doi.org/10.1016/j.ces.2012.11.024
29 Möller, A., Eschrich, R., Reichenbach, C., Guderian, J., Lange, M., Möllmer, J.: Dynamic and equilibrium-based investigations of CO_2-removal from CH_4-rich gas mixtures on microporous adsorbents. Adsorption **23**(2–3), 197–209 (2017). https://doi.org/10.1007/s10450-016-9821-x
30 Parinyakit, S., Worathanakul, P.: Static and dynamic simulation of single and binary component adsorption of CO_2 and CH_4 on fixed bed using molecular sieve of zeolite 4A. Processes **9**(7), 1250 (2021). https://doi.org/10.3390/pr9071250
31 Silva, J.A., Schumann, K., Rodrigues, A.E.: Sorption and kinetics of CO_2 and CH_4 in binderless beads of 13X zeolite. Microporous Mesoporous Mater. **158**, 219–228 (2012). https://doi.org/10.1016/j.micromeso.2012.03.042
32 Silva, J.A., Cunha, A.F., Schumann, K., Rodrigues, A.E.: Binary adsorption of CO_2/CH_4 in binderless beads of 13X zeolite. Microporous Mesoporous Mater. **187**, 100–107 (2014). https://doi.org/10.1016/j.micromeso.2013.12.017
33 Kretzschmar, A., Selmert, V., Weinrich, H., Kungl, H., Tempel, H., Eichel, R.-A.: Tailored gas adsorption properties of electrospun carbon nanofibers for gas separation and storage. ChemSusChem **13**(12), 3180–3191 (2020). https://doi.org/10.1002/cssc.202000520

34 Kretzschmar, A., Selmert, V., Weinrich, H., Kungl, H., Tempel, H., Eichel, R.-A.: Study of CO_2 sorption kinetics on electrospun polyacrylonitrile-based carbon nanofibers. Chem. Eng. Technol. **44**(7), 1168–1177 (2021). https://doi.org/10.1002/ceat.202000463

35 Selmert, V., Kretzschmar, A., Weinrich, H., Tempel, H., Kungl, H., Eichel, R.-A.: CO_2/N_2 separation on highly selective carbon nanofibers investigated by dynamic gas adsorption. ChemSusChem **15**(14), e202200761 (2022). https://doi.org/10.1002/cssc.202200761

36 Park, J., Kretzschmar, A., Selmert, V., Camara, O., Kungl, H., Tempel, H., Basak, S., Eichel, R.A.: Structural study of polyacrylonitrile-based carbon nanofibers for understanding gas adsorption. ACS Appl. Mater. Interfaces **13**(39), 46665–46670 (2021). https://doi.org/10.1021/acsami.1c13541

37 Schierholz, R., Kröger, D., Weinrich, H., Gehring, M., Tempel, H., Kungl, H., Mayer, J., Eichel, R.-A.: The carbonization of polyacrylonitrile-derived electrospun carbon nanofibers studied by in situ transmission electron microscopy. RSC Adv. **9**(11), 6267–6277 (2019). https://doi.org/10.1039/C8RA10491C

38 Borowec, J., Selmert, V., Kretzschmar, A., Fries, K., Schierholz, R., Kungl, H., Eichel, R.-A., Tempel, H., Hausen, F.: Carbonization-temperature-dependent electrical properties of carbon nanofibers-from nanoscale to macroscale. Adv. Mater. **35**(31), e2300936 (2023). https://doi.org/10.1002/adma.202300936

39 Grubner, O., Jírů, P., Rálek, M.: Molekularsiebe. VEB Deutscher Verlag der Wissenschaften, Berlin (1968)

40 Basmadjian, D.: Rapid procedures for the prediction of fixed-bed adsorber behavior. 1. Isothermal Sorption of single gases with arbitrary isotherms and transport modes: Principles and recommended methods. Ind. Eng. Chem. Process. Des. Dev. **19**, 129–137 (1980)

41 Glueckauf, E., Coates, J.I.: Theory of chromatography. The influence of incomplete equilibrium on the front boundary of chromatograms and on the effectiveness of separation. J. Chem. Soc. (1947). https://doi.org/10.1039/JR9470001315

42 Myers, A.L., Prausnitz, J.M.: Thermodynamics of mixed-gas adsorption. AIChE J. **11**(1), 121–127 (1965). https://doi.org/10.1002/aic.690110125

43 Wilkins, N.S., Rajendran, A.: Measurement of competitive CO_2 and N_2 adsorption on zeolite 13X for post-combustion CO_2 capture. Adsorption **25**(2), 115–133 (2019). https://doi.org/10.1007/s10450-018-00004-2

44 Wilkins, N.S., Sawada, J.A., Rajendran, A.: Measurement of competitive CO_2 and H_2O adsorption on zeolite 13X for post-combustion CO_2 capture. Adsorption **26**(5), 765–779 (2020). https://doi.org/10.1007/s10450-020-00199-3

45 Wilkins, N.S., Rajendran, A., Farooq, S.: Dynamic column breakthrough experiments for measurement of adsorption equilibrium and kinetics. Adsorption **27**(3), 397–422 (2021). https://doi.org/10.1007/s10450-020-00269-6

46 Walton, K.S., Sholl, D.S.: Predicting multicomponent adsorption: 50 years of the ideal adsorbed solution theory. AlChE J. **61**(9), 2757–2762 (2015). https://doi.org/10.1002/aic.14878

47 Liang, W., Liu, Z., Peng, J., Zhou, X., Wang, X., Li, Z.: Enhanced CO_2 adsorption and $CO_2/N_2/CH_4$ selectivity of novel carbon composites CPDA@A-Cs. Energy Fuels **33**(1), 493–502 (2019). https://doi.org/10.1021/acs.energyfuels.8b03637

48 Hamon, L., Jolimaître, E., Pirngruber, G.D.: CO_2 and CH_4 separation by adsorption using Cu-BTC metal–organic framework. Ind. Eng. Chem. Res. **49**(16), 7497–7503 (2010). https://doi.org/10.1021/ie902008g

49 Rainone, F., D'Agostino, O., Erto, A., Balsamo, M., Lancia, A.: Biogas upgrading by adsorption onto activated carbon and carbon molecular sieves: experimental and modelling study in binary CO_2/CH_4 mixture. J. Environ. Chem. Eng. **9**(5), 106256 (2021). https://doi.org/10.1016/j.jece.2021.106256

50 Rocha, L.A., Andreassen, K.A., Grande, C.A.: Separation of CO_2/CH_4 using carbon molecular sieve (CMS) at low and high pressure. Chem. Eng. Sci. **164**, 148–157 (2017). https://doi.org/10.1016/j.ces.2017.01.071

51 Peredo-Mancilla, D., Ghimbeu, C.M., Ho, B.-N., Jeguirim, M., Hort, C., Bessieres, D.: Comparative study of the CH_4/CO_2 adsorption selectivity of activated carbons for biogas upgrading. J. Environ. Chem. Eng. **7**(5), 103368 (2019). https://doi.org/10.1016/j.jece.2019.103368